Intraspecific variation in growth-related traits—from leaf to whole-tree—in three provenances of Cryptomeria japonica canopy trees grown in a common garden

Azuma, Wakana A.

Kawai, Kiyosada

Tanabe, Tomoko

Nakahata, Ryo

Hiura, Tsutom

(Citation)
Ecological Research,38(1):83-97

(Issue Date)
2023-01

(Resource Type)
journal article

(Version)
Accepted Manuscript

Special features "Functional biogeography: Lessons from the geographic variations in the most dominant tree species in Japan"

Intraspecific variation in growth-related traits—from leaf to whole-tree—in three provenances of *Cryptomeria japonica* canopy trees grown in a common garden

WAKANA A. AZUMA[1, 2, †, *]

KIYOSADA KAWAI [3, 4, †]

TOMOKO TANABE[5]

RYO NAKAHATA[2, 6]

TSUTOM HIURA[7]

[1] Graduate School of Agricultural Science, Kobe University, Kobe 657-8501, JAPAN

[2] Graduate School of Agriculture, Kyoto University, Kyoto 606-8502, JAPAN

[3] Center for Ecological Research, Kyoto University, Otsu 520-2113, JAPAN

[4] Forestry Division, Japan International Research Center for Agricultural Science (JIRCAS), Tsukuba 305-8686, JAPAN

[5] Graduate School of Global Environmental Studies, Kyoto University, Kyoto, 606-8501,

JAPAN

[6] Graduate School of Agricultural and Life Sciences, The University of Tokyo, 113-8657, JAPAN

[7] Department of Ecosystem Studies, The University of Tokyo, Tokyo, 113-8657, JAPAN

† WAA and KK should be considered joint first author.

*Corresponding author: Email: wakana@port.kobe-u.ac.jp, Phone: +81-78-803-5936

Abstract

To elucidate the physiological and morphological factors underlying intraspecific variation in growth rate, we examined the variation in leaf and whole-tree traits for three geographical variations of ca. 45-year-old Japanese cedar (*Cryptomeria japonica* D. Don) with contrasting heights and radial growth in a common garden. Traits that reflect leaf-level photosynthesis, water relations, and whole-tree level crown structure in relation to light use and hydraulic architecture were measured. Overall, intraspecific variation in growth characteristics in field-grown adult trees was regulated by whole-tree properties rather than leaf properties. Most leaf traits were similar among provenances. Nevertheless, the leaf traits exhibited highest maximum net photosynthetic rate, dark respiration rate, and light compensation point in provenances whose native habitats are most similar to the common garden in the present study. Together with previous reports that this provenance has higher root nutrient acquisition capacity than the other two provenances, it can be said that organ-level resource use strategies are coupled in a tandem manner. At the whole-tree level, hydraulic architecture—as explained by axial variation in the hydraulically-weighted tracheid diameter—can be linked to leaf distribution with respect to light use strategies as well as water transport capacity, leading to differences in growth characteristics among provenances. The study of intraspecific variation in growth

characteristics in trees with a wide range of native habitats is expected to be a useful indicator for predicting changes in growth potential and forest dynamics in response to climate change in each habitat.

Keywords: xylem anatomy, functional trait, photosynthesis, transpiration, hydraulic architecture

Introduction

The patterns and mechanisms of tree growth have long been the core research topics in tree physiology. The rate of tree growth is influenced by 1) the inherited characteristics of trees, such as size, phenology, and physiological properties (e.g., Kitajima 1994; Moreira et al. 2014; Obeso 2002; Poorter and Remkes 1990); 2) the surrounding abiotic and biotic factors, such as light availability, mycorrhizal symbiosis, and herbivore pressure (Coley and Barone 1996; Montgomery and Chazdon 2002; Wu and Xia 2006); and 3) their interactions (Nabeshima et al. 2010). To understand the mechanisms underlying the variation in the growth rate of trees, Hunt (1978) introduced the concept of growth analysis, where dry mass-based relative growth rate (RGR) is expressed as the net assimilation rate (NAR) multiplied by the leaf area ratio (LAR, total leaf area per unit whole-plant mass). This equation indicates that tree growth is governed by both leaf-level photosynthetic rate and whole-tree carbon allocation. Therefore, it is expected that any plant traits (physiological and morphological characteristics) influencing NAR and LAR could potentially cause variation in growth rate.

Water transport from the roots to leaves is a major determinant of photosynthetic capacity—and thus possibly NAR—because CO_2 absorption inevitably induces water loss due to transpiration (Brodribb 2009; Sperry 2003). Previous studies have demonstrated that organ-level hydraulic conductivity strongly influences the maximum photosynthetic rate (Brodribb and Feild 2000; Santiago et al. 2004) and growth rate (Fan et al. 2012; Hietz et al. 2017; Poorter et al. 2010). Hydraulic conductivity is governed by the morphology, dimensions (particularly the diameter), and spatial arrangements of the conducting elements (vessels and tracheids) (Hacke et al. 2017; Tyree and Zimmermann 2002). The diameter of conducting elements varies according to tree size (Olson et al. 2014), environmental gradients (Arenas-Navarro et al. 2021, Zheng et al. 2022), and position within trees (Petit et al. 2008; Spicer and Gartner 2001). The latter factor determines the pattern of accumulation of hydraulic resistance along tree height, thus influencing whole-tree hydraulic conductivity, especially in large trees (Liu et al. 2019). Theoretical (Enquist 2003; West et al. 1999) and empirical (Anfodillo et al. 2006, 2013; Olson et al. 2018; Williams et al. 2019) studies have shown that the diameter of conducting elements increases from the stem tip to the base as $D = \alpha L^{\beta}$, where D is the conduit diameter, L is the distance from the tree apex, and α and β are coefficients. This increase in diameter possibly mitigates the negative effects of accumulating hydraulic resistance on tree growth and photosynthesis (Ryan and Yoder 1997). Here, if $\beta \geq 0.20$, metabolic theory predicts that accumulated hydraulic resistance would be nearly independent of L; in such cases, trees can maintain their metabolism with an increase in height (Enquist 2003; West et al. 1999). Accordingly, the variations in α and β should reflect the differences in whole-tree hydraulic architecture, and thus the growth rate (Rosell et al. 2017).

In addition to leaf-level photosynthetic capacity, the LAR also affects the RGR of trees (Givnish 1988; Kitajima 1994; Poorter and Remkes 1990). The LAR can be further decomposed into specific leaf area (SLA) multiplied by the leaf mass fraction (LMF, leaf mass per unit whole-tree mass). Therefore, both leaf morphology and carbon allocation to leaves influence the LAR. Leaf dry mass per area (LMA, the inverse of SLA) is often negatively correlated with RGR across species (e.g., Gibert et al. 2016; Iida et al. 2014; Poorter et al. 2006). With regard to LMF, biomass distribution among organs reflects the volume and density of each organ (leaves, stems, branches, and roots). Large trees (> 1,000 kg) generally allocate most of the biomass (> 70%) to stem wood (Poorter et al. 2015). Therefore, for a given amount of photosynthate and SLA, an increase in wood density at the stem increases biomass allocation to the stem (King et al. 2006), thus reducing LMF and RGR. At the whole-tree level, high allocation of biomass to stems reduces LAR, and thus constrains RGR (Onoda et al. 2014).

To date, attempts to identify the traits underlying the RGR of trees in relation to NAR and LAR have focused on interspecific variation, mostly using different phylogenies (e.g., King et al. 2006; Martínez-Vilalta et al. 2010; Poorter and Remkes 1990; Wright et al. 2010). However, few studies have dealt with intraspecific variations. Because evolutionary processes do not produce extreme phenotypes at smaller temporal scales, intraspecific trait variation is often similar to or lower than interspecific variations (e.g., Asner et al. 2014; Messier et al. 2010). Investigating such within-species variations requires the following: 1) establishing the evolutionary robustness of trait–growth relationships, and 2) investigating an extensive suite of traits that may contribute to a mechanistic and comprehensive understanding of tree growth (Medeiros et al. 2019). Although the importance of LAR-associated traits (e.g., LMA and wood density) on growth is well appreciated, few studies have examined them together with leaf-level physiological traits, particularly for field-grown large trees. In practical terms, this type of within-species approach is ideal for species that show wide distribution ranges—including heterogeneous resource availabilities—because variation in local environments would cause divergent selections in traits and associated growth rates, providing opportunities to test their evolutionary correlations (Cavender-Bares 2019). The Japanese archipelago is a suitable area for this type of study, as it encompasses a wide environmental gradient that causes high intraspecific variation in phenotypic traits (e.g., Ishii et al. 2018; Osada et al. 2015; Tateishi et al. 2010).

Here, we chose the natural geographical variations of the Japanese cedar (*Cryptomeria japonica* D. Don), which dominates about 20% (including plantation forests) of Japan's forest area (Forestry Agency of Japan 2011) as a study clade. We examined the intraspecific variations in leaf and whole-tree traits associated with NAR and LAR in relation to their growth rate in a common garden. *C. japonica* is widely distributed in the Japanese archipelago (from 30°15′ N to 40°42′ N) and comprises genetically differentiated provenances (Tsumura et al. 2012, 2014) that differ in morphology, growth rate, allometries, and other functional traits (Hiura et al. 2021; Nishizono et al. 2014; Osone et al. 2021). Thus, this species is ideal for testing trait−growth relationships at the intraspecific level. A previous study conducted in the same common garden had shown that the root exudation rate and nutrient status of leaves and roots were higher in provenances with a high growth rate, indicating that adaptive divergence in nutrient-uptake strategies among provenances causes a difference in growth rates (Ohta et al. 2019). Based on this, we tested the prediction that provenances in which leaf and whole-tree traits are associated with high NAR (e.g., high photosynthetic rate, conductive tracheid, and high nitrogen content) and high LAR (e.g., low LMA, low wood density, and high fraction of leaf mass) show high RGR in terms of height and diameter. We measured 25 leaf and whole-tree traits that are associated with NAR and LAR through their influence on the resource use strategies of light, water, and nutrients (e.g., leaf photosynthetic rate, crown structure, and tree hydraulic architecture). Using these data, we compared the traits among three provenances of ca. 45-year-old *C. japonica* with different genotypes and contrasting RGR grown under the same environment.

Methods

Study site and plant materials

The study was conducted in a common garden of *C. japonica* established at the Wakayama Experimental Forest of Hokkaido University in Wakayama Prefecture, Japan (33°40′ N, 135°40′ E, and 240 m above sea level). This forest is covered by a very thin and weakly developed mineral soil without horizon differentiation (Regosol, based on the World Reference Base for Soil Resources) (Kanda et al. 2018). The mean annual precipitation and temperature from 1985 to 2019 were 3,564 mm and 14.7°C, respectively (Japan Meteorological Agency).

The common garden was located on a south-facing slope, and the soil color (gray), texture (silt and gravel), and depth (< 10 cm) were uniform across the slope. In the common garden, *C. japonica* grown in various regions of Japan were planted with similar densities (ca. 2,000 individuals per hectare) between 1967 and 1973. The stand had not been managed after planting until our field survey, and the canopy was closed without any gaps. Here, we used clonal stands of the three provenances that had also been used in Ohta et al. (2019): Yoshino, Yanase, and Yaku. These provenances were planted within 50 m of each other at the upper, middle, and lower parts of the slope, respectively. The native habitats of all three provenances are located in the southwestern part of Japan (Figure 1). As in the common garden, all native habitats are covered with very thin soils due to high precipitation and steep slopes, but the basement rock of each native habitat is different (sedimentary rock in Yoshino, sandstone and shale in Yanase, and granite in Yaku) (Geological Survey of Japan 2015). Yoshino and Yanase are known to have relatively high growth rates in the early stage of growth (< ca. 50 years old), whereas Yaku has low growth rates (Itaka et al. 2013; Nishizono et al. 2014). These growth patterns were also observed in the mean tree height and diameter at breast height (DBH) of each provenance measured across the common garden of the present study in 2015: 18.3 m and 23.1 cm in Yoshino (n = 100), 15.4 m and 19.2 cm in Yanase (n = 193), and 10.9 m and 18.6 cm in Yaku (n = 119), respectively. The age of stands from each provenance in 2015 was 49 years in Yaku, 46 years in Yanase, and 43 years in Yoshino.

In this study, three individuals of each provenance were cut down from their stem base at noon on a sunny day in August 2018 and used for the measurements described below. The canopy tops of each sample tree were exposed to direct sunlight. We stretched a tape measure along the stem to measure the tree height, crown depth, and height and diameter of the primary branches attached to the stem of each individual, except for one Yaku tree. The mean height and DBH of the sample trees for each provenance were 21.1 m and 22.7 cm in Yoshino, 20.9 m and 25.6 cm in Yanase, and 11.8 m and 15.7 cm in Yaku, respectively. To calculate the stem volume of each individual, stem disks (approximately 1 cm in thickness) were collected at 5 m intervals starting from a height of 1.3 m along the stem. The diameters were recorded, and the stem volume was calculated as the sum of the truncated cones.

Growth characteristics and tree structures

To estimate the recent growth characteristics of each provenance, the annual stem height and radial growth rates (G_h and G_r, cm yr^{-1} and mm yr^{-1}) from 2013 to 2016 were measured from the annual shoot length at the top of each tree crown (except for one individual from Yoshino, which could not be measured because the tip of the trunk was unclear). These measurements were recorded with an accuracy of 1 mm. The annual ring width was measured from one direction of the stem disk at a height of 1.3 m with an accuracy of 0.001 mm. Based on the above data, we calculated the relative growth rate for height (RGR_h, yr^{-1}) and DBH (RGR_r, yr^{-1}) from 2013 to 2016 using the following equation (Hunt 1982), assuming that both show exponential growth:

$$\frac{\ln(X_j)-\ln(X_i)}{t_j-t_i} \qquad \text{Eqn. 1}$$

where X_j and X_i are the height or DBH at times j and i, respectively (when annual growth ceases), and t_j and t_i are the years. G_h, G_r, RGR_h, and RGR_r were calculated for each year-interval (2013–2014, 2014–2015, 2015–2016) for individual trees.

One woody core (ca. 3 cm in length from the cambium) was collected from the main stem at DBH using an incremental borer (5.15 mm in diameter; Haglöf, Langsele, Sweden) from 10–12 individuals per provenance in August 2019. This woody core was used to calculate the sapwood density (WD, g cm^{-3}). The sapwood volume was measured from the diameter and length of a core (assuming a cylindrical shape), and the bark and heartwood portions (based on the visual check) were removed with a razor blade before measurement. All samples were oven-dried (65°C, > 72 h), and their dry masses were recorded. The volumetric density of the sapwood was then calculated as the dry mass divided by its fresh volume.

The crown architecture was evaluated by the absolute crown depth (CD, m), and the ratio of CD to tree height (RCD, m m^{-1}) was calculated for each individual. In addition, we assumed a pipe model, in which the ratio of leaf area to the cross-sectional area of the branch base is constant (Shinozaki et al. 1964). Based on this, we calculated the total cross-sectional area per stem volume (TBA, cm^2 m^{-3}) of primary branch bases for each individual as an alternative index of LAR.

Tree hydraulic architecture

To analyze the stem anatomy, we excised one sample from the cambium (approximate length, 2 cm; width, 1 cm; depth, 1–2 cm) from all the stem disks we collected, avoiding the reaction wood part. Subsequently, transverse sections (approximate thickness, 30–40 μm) were prepared using a sliding microtome (Figure 2). The samples were stained with 0.5% (w/v) safranin in 50% ethanol and dehydrated using an ethanol series (50%, 99.5%, and 100%). Finally, the samples were dehydrated in xylene and mounted on glass slides with Canada balsam. Images were captured using a digital camera (EOS kiss X3, Canon, Tokyo, Japan) coupled to a light microscope (BX50, Olympus, Tokyo, Japan). The resolution of the images was 1919 pixels mm^{-1} with a full size of approximately 1.2 mm × 0.8 mm. Using these images, we measured the tracheid density (TD, mm^{-2}) of earlywood and the mean tracheid lumen area (TLA, $μm^2$) for > 650 tracheids per image using the Fiji image processing software (Schindelin et al. 2012). The disjunction between earlywood and latewood followed Mork's definition (Denne 1988): latewood was defined as the wood with the ratio of lumen diameter and double wall thickness < 2. The TLA was convened to the tracheid diameter (D, μm) by assuming circular cross-sections, and the mean hydraulically-weighted tracheid diameter (D_h, μm) of every stem disk was calculated as follows (Tyree and Zimmermann 2002):

$$D_{\mathrm{h}} = \left(\frac{1}{n}\sum_{i=1}^{n} D^4\right)^{\frac{1}{4}} \qquad \text{Eqn. 2}$$

where n is the number of tracheids.

In a soil–plant hydraulic continuum, water flow occurs in proportion to the water potential gradient and is inversely proportional to the hydraulic conductivity according to Darcy's law (Sperry et al. 1998). To estimate the potential water flow in the whole tree, we calculated the water potential gradient from the difference between Ψ_{TL} and Ψ_R, as described below. The potential specific xylem conductivity at a certain height (K_p, kg m^{-1} s^{-1} MPa^{-1}) was calculated according to (Poorter et al. 2010):

$$K_{\mathrm{p}} = \left(\frac{\pi \rho w}{128\eta}\right) TD * D_h^4 \qquad \text{Eqn. 3}$$

where ρ_w is the density of water at 20°C (998.2 kg m^{-3} at 20°C), η is the viscosity of water at 20°C (1.002×10^{-3} Pa s at 20°C), and TD and D_h are as described above.

We calculated K_p at different heights from every stem disk, and then the axial variation-weighted potential specific xylem conductance (K_{ap}, kg m^{-2} s^{-1} MPa^{-1}) and potential transpiration rate per unit sapwood area (E_p, kg m^{-2} s^{-1}) were estimated. Because of the decrease in D_h from the stem base to the treetop (Figure S1a), K_p decreased as sampling height increased in each tree, and its variation was relatively well explained by linear regressions (R^2 = 0.53–1.00, Figure S1b). These patterns allow us to express the minimum specific resistivity (R_{min}, an inverse of K_p) as a function of height as follows:

$$R_{\mathrm{min,i}} = \frac{1}{a_i H + b_i} \quad \text{Eqn. 4}$$

where $R_{min,i}$ H, a_i, and b_i are the R_{min}, height, and coefficients of tree i, respectively. Integrating R_{min} from the ground to the individual tree height yielded the minimum cumulative specific resistivity of the stem (R_{cum_min}, m^2 s MPa kg^{-1}), and potential specific xylem conductance (K_{ap}) was calculated as the inverse of R_{cum_min}. The E_p was calculated as K_{ap} multiplied by the water potential gradient from the roots to the treetop ($\Psi_R - \Psi_{TT}$, MPa). The above calculations assumed that most water movements occur in the earlywood at the outermost sapwood where large tracheids are observed; thus, we considered our results to be robust to the radial variation of tracheid anatomy.

Leaf water relations

After cutting down the trees in the common garden as described above, the daytime water potential of treetop leaves (Ψ_{TL}, MPa), lowest-crown leaves (Ψ_{LL}, MPa), and fine roots (Ψ_R, MPa) were immediately measured for three replicates per individual using a pressure chamber (Model 1000, PMS Instruments, Corvallis, USA). Branches (ca. 30 cm in length) were sampled from the treetop of each individual, immediately recut in bucketed water, and covered with a black plastic bag overnight in the laboratory for the pressure–volume measurement.

The pressure–volume curve of the leaves (second- and current-year internodes; three shoots per provenance) was obtained using the bench-drying approach for the pressure–volume technique (Tyree and Hammel 1972). Using a pressure chamber (Model 1000, PMS Instruments, Corvallis, USA), we repeatedly measured the leaf water potential (Ψ_L, MPa) and fresh mass (M_F, g) of the sampled leaves (repeat pressurization method, Hinckley et al. 1980, Parker and Colombo 1995). After the pressure–volume measurement, all the sample shoots were photographed to measure the total leaf surface area (A_L, m^2), as described below. Next, the leaves were oven-dried to constant weight at 65°C for 48 h to obtain the leaf dry mass (M_D, g). To estimate the drought tolerance of shoots, we calculated the osmotic potential at saturation (Ψ_{sat}, MPa), osmotic potential at turgor loss (Ψ_{tlp}, MPa), and relative water content at turgor loss (RWC_{tlp}) at the bulk shoot level using the pressure–volume curve. The saturated leaf water content (M_W = MF – MD) was used to calculate leaf hydraulic capacitance (C_L, mol m^{-2} MPa^{-1}) and succulence (S_L, g H_2O m^{-2}).

$$C_L = (\delta RWC/\delta \Psi_L)\ (M_D/A_L)\ (M_W/M_D)\ /\ MW \qquad \text{Eqn. 5}$$

$$S_L = M_W/A_L \qquad \text{Eqn. 6}$$

where $\delta RWC/\delta \Psi_L$ is the slope of the Ψ_L–RWC relationship calculated from the pressure–volume curve before the turgor loss point, and MW is the molecular weight of water.

Leaf morphology

After the pressure–volume measurement, each sample shoot (three shoots per provenance) was placed on a slide viewer, illuminated from below, and photographed to obtain the shoot silhouette images. All leaves were detached from the shoot axis, laid on the slide viewer without overlap, and photographed. The photographs of the shoots and leaves were analyzed using the ImageJ image analysis software (Schneider et al. 2012) to quantify the shoot silhouette area (A_S, m^2) and projected leaf area (A_P, m^2). To obtain A_L, the perimeter-to-width ratios obtained from the transverse sections of leaves were multiplied by A_P (Azuma et al. 2016). We calculated the leaf mass per area (LMA = M_D/A_P, g m^{-2}) and shoot silhouette area to projected leaf area ratio (SPAR = A_S/A_P, a measure of leaf overlap within the shoot).

Leaf photosynthetic traits

In August 2019, we sampled a branch (approximate length, 30 cm) from the treetop of each individual tree using a long sickle. The branch was immediately recut under water and fully rehydrated in the laboratory for photosynthetic measurement. The gas exchange of second-year shoots was measured in all sampled branches (three branches per provenance) using the LI-6400 portable gas exchange system fitted with an LI-6400-05 conifer chamber (Li-Cor Inc., Lincoln, NE, USA). The air temperature and CO_2 concentration in the cuvette were maintained at 25°C and 380 ppm, respectively. We used an external halogen-type light source fitted with a profile spot projection lens (MHAB-150W and ML-50, Moritex Corp., Tokyo, Japan) to provide parallel beam radiation with a maximum photosynthetic photon flux density (PPFD) of 1600 μmol m^{-2} s^{-1}. We varied the light intensity to obtain the photosynthetic light response curve for each shoot.

Following these measurements, the leaves inside the conifer chamber (10 cm^2) were carefully cut out and photographed to measure the projected leaf area using Image J (Schneider et al. 2012). The leaves were then oven-dried to a constant mass to determine the leaf dry mass. We estimated maximum net photosynthetic rate (P_{max}, μmol CO_2 m^{-2} s^{-1}), dark respiration rate (R, μmol CO_2 m^{-2} s^{-1}), and light compensation point (L_C, μmol m^{-2} s^{-1} PPFD) from the relationship between light intensity and net photosynthetic rate.

These measurements were conducted using the Light Response Curve software developed by Li-Cor Inc. (Norman et al. 1992). We also calculated maximum photosynthetic rate per leaf dry mass (P_{max_mass}, nmol CO_2 g^{-1} s^{-1}) by dividing P_{max} by LMA.

To evaluate the long-term photosynthetic water-use efficiency, we measured the leaf carbon isotope ratio ($\delta^{13}C$, ‰) in 9–10 individuals of each provenance from which we had collected stem cores (Farquhar et al. 1989). The leaves were oven-dried (65°C, > 72 h) and then ground using a mill. Then, $\delta^{13}C$ was measured using an isotope ratio mass spectrometer (DELTA V Plus and DELTA V Advantage, Thermo Fisher Scientific, Massachusetts, USA) at the Center for Ecological Research (CER), Kyoto University. Simultaneously, the dry mass-based leaf nitrogen and carbon concentrations (N_{mass} and C_{mass}, %) were measured using an elemental analyzer (Flash 2000, Thermo Fisher Scientific) coupled to an isotope ratio mass spectrometer.

Statistical analysis

All analyses were performed using R (R Core Team 2019, R version 3.6.1). To calculate K_{ap} and E_p, we first estimated coefficients *a* and *b* in Eqn. 4 for each tree with nonlinear least square regression analyses using the R function 'nls'. Using these values, we integrated Eqn. 4 from 0 (ground) to tree height for each tree to yield R_{cum_min} using the ‘integrate’ function in the R package ‘stats’ (version 4.1.2).

To examine the differences in the leaf, stem, and whole-tree traits among provenances, we used one-way ANOVA followed by Tukey’s HSD post hoc tests. We also examined the residual plots of linear regressions for each trait. When the data did not meet the assumptions of ANOVA (normality and homogeneity of variances), we instead conducted the Kruskal–Wallis test followed by the Steel–Dwass test. To compare G_h, Gr, RGR_h, and RGR_r, we first calculated the average provenance-by-year values to consider the variation in growth among years, and then examined the differences among provenances based on the linear mixed model analyses with a restricted maximum likelihood (REML) estimation, where provenance was fixed effect and year was a random intercept, using the R package ‘lme4’ (Bates et al. 2015). Following this, we examined the differences among provenances using linear mixed model analyses (with provenance as a fixed effect and year being a random intercept) using the R package ‘lme4’ (Bates et al. 2015). The model parameters were calculated by REML estimation.

To examine the axial variation of D_h, we converted the sampling height to the distance from the tree apex (L), thus enabling comparisons among trees of different heights. We estimated the slope (basipetal conduit widening rate, β) and intercept (log D_h at 1 m below the treetop, α) of L–D_h relationships among provenances based on linear mixed model analyses, where L, provenance, and their interaction were fixed effects and individual trees had a random intercept. The model parameters were calculated using REML estimation. Here, we $\log_{10}$-transformed D_h and L prior to analyses to reflect the scaling relationship of D_h with L (see Introduction). The same analysis was performed by substituting L with the relative distance from the treetop or stem diameter at sampling height to estimate the effect of size differences among provenances on tracheid tapering. We also calculated marginal and conditional R^2 (R_m^2 and R_c^2, respectively, Nakagawa and Schielzeth 2013) to evaluate the model fit using the R package 'MuMIN' (Barton 2016). We set a significance level of 0.05.

Results

Growth characteristics and tree structures

G_h, G_r, RGR_h, and RGR_r were the lowest in the Yaku provenance, followed by Yoshino and Yanase (Table 1). Correspondingly, WD was highest in Yaku, followed by Yoshino, and then Yanase (Table 2). CD was larger in Yanase than in Yaku. RCD was not significantly different among the provinces; however, there was a trend of Yanase having a higher RCD compared to the other two provenances (Table 2). TBA was significantly higher in Yaku than in Yanase and Yoshino.

Axial variation of tracheid diameter and whole-tree hydraulics

For all provenances, the D_h was generally smallest near the top of the tree, and the largest D_h was found near the stem base (Figure 3, Table 3). The slope (basipetal conduit widening rate, β) and intercept (log D_h at 1 m below the treetop, α) in the L–D_h relationship were significantly different between provenances (Table 3): β was higher in Yanase and Yoshino than in Yaku, whereas α was higher in Yaku than in the other two. Yanase had a marginally higher β than Yoshino ($p = 0.076$). In addition, provenances with high β tended to exhibit low α. The overall model fit was relatively good (both R_m^2 and $R_c^2 = 0.85$). We also found that on average, provenances with higher β had longer CD ($R^2 = 0.999$, $p = 0.021$, $n = 3$), indicating a link between hydraulics and crown architectures at the whole-tree level (Figure 3). However, when we substituted L with the relative distance from the tree top or stem diameter at the sampling height, the slope was not significantly different among provenances in either case (R_m^2 and $R_c^2 = 0.73$, Table S1, for relative distance; $R_m^2 = 0.72$, $R_c^2 = 0.76$, Table S2 for diameter). This suggested that the results in the L–D_h relationship may reflect different sizes among provenances.

A decline in D_h caused a decline in K_p along tree height with indistinguishable slopes among provenances ($p = 0.77$, Figure S1). These patterns led to significant positive correlations between total tree height and R_{cum_min} across trees (p = 0.003, Figure S2). Consequently, despite having the lowest β, Yaku had the highest K_{ap} because it also had the lowest tree height. Despite the high K_{ap} in Yaku, E_p was not significantly different among provenances (p = 0.28), as it was offset by the relatively small $\Psi_{TL} - \Psi_R$ in Yaku (Table 2).

Leaf water relations, morphology, and photosynthetic traits

Leaf water relations and leaf morphology were similar, with no significant differences among provenances (Table 2). Although most leaf photosynthetic traits were not significantly different between provenances, there were significant or marginally significant differences in R (p = 0.042), Lc (p = 0.053), and $\delta^{13}C$ (p = 0.054) among provenances. R and Lc were highest in Yoshino and lowest in Yanase, whereas $\delta^{13}C$ was highest in Yaku and lowest in Yanase (Table 2).

Discussion

Here, we compared the traits of three provenances of ca. 45-year-old *C. japonica* with different genotypes and contrasting RGR (Yaku, Yanase, and Yoshino) grown under the same environment. Our results partially supported our prediction that the trees in the resource-acquisitive provenance achieved higher growth rates. Among the traits affecting NAR and LAR that lead to differences in RGR, leaf traits had similar values among provenances, whereas canopy structure and hydraulic architecture at the whole-tree level were different between provenances.

The life-history theory suggests that organ-level resource use strategies are coupled in a tandem manner (Grime et al. 1997; Reich 2014). The previous studies conducted in the same common garden showed the highest rate of root exudation in Yoshino whose native habitat was most similar to the common garden (Ohta et al. 2019). It has been speculated that this is a result of adaptation to the basement rock in its native habitat. In support of the life-history theory, Yoshino showed resource-acquisitive leaf traits, such as the highest P_{max}, R, and L_c among the three provenances in the present study (Table 2). In turn, the lowest Lc in Yanase may allow Yanase to distribute their leaves in the lowest position relative to tree height. In *C. japonica*, photosynthetic parameters such as P_{max}, V_{cmax}, and nitrogen content in the second-year (former current year) shoots decrease after summer and primary photosynthetic sites shift to current-year shoots as the seasons changed (Inoue et al. 2018, Kobayashi et al. 2010, Tobita et al. 2014). Considering that the P_{max} in the present study was measured on the second-year shoots, it would be reasonable that P_{max} was lower than that measured on the current year shoots of

C. japonica in general (Osone et al. 2021). P_{max} was similar among provenances, but the leaf water-use efficiency (estimated by $\delta^{13}C$) tended to be higher in Yaku with lower growth rate (Table~~s~~ 1 and 2). Leaf water-use efficiency estimated by $\delta^{13}C$ represents long-term accumulation of the photosynthesis per unit stomatal conductance (Farquhar et al. 1989). The high leaf water-use efficiency in Yaku may be partially due to low basipetal conduit widening rate (β), which negatively affects photosynthesis and growth at the whole-tree level through the accumulation of hydraulic resistance from stem anatomical traits as discussed below. However, most leaf water relations, morphology, and photosynthetic traits were similar among provenances (Table 2), indicating that growth-related traits at the leaf level alone did not describe differences in RGR among provenances.

In terms of growth characteristics, Yaku trees showed the lowest stem height, radial growth rate, and RGR, corresponding to the highest sapwood density (Tables 1 and 2). The high WD in Yaku was also associated with a small tracheid diameter at the same height compared to the two other provenances (Figure S1a). WD is negatively related to volumetric growth and positively related to strength (e.g., van Gelder et al. 2006; Poorter et al. 2003); therefore, the high WD in Yaku may represent a genetically differentiated trait in response to the limited tree size due to typhoon-induced canopy disturbance in its native habitat (Ishii et al. 2010; Takashima et al. 2009). In addition, WD can influence LAR, which is related to tree growth rate (Givnish 1988; Kitajima 1994; Poorter and Remkes 1990). High biomass allocation to the stem affected the variation in WD and could be predicted to reduce LAR, leading to constrained RGR (Poorter et al. 2010; Wright et al. 2010). However, the large TBA in Yaku (Table 2) indicated that assuming a pipe model, the biomass allocation to leaves was higher (Shinozaki et al. 1964) when assuming no difference in leaf area relative to the cross-sectional area of the branch base among provenances. However, the foliage was concentrated at a relatively higher position on the stem. Coniferous trees generally allow light to penetrate deeper into the canopy compared to broadleaf trees because of the arrangement of shoots and branches (Ishii and Asano 2010). Multi-layered trees with branches distributed throughout the crown typically show lower efficiency of light interception compared to that in single-layered trees with branches distributed in the upper canopy. However, the productive leaf area is theoretically maximized by maintaining a deep canopy in conifer trees (Onoda et al. 2014; Niinemets 2010; Stenberg 1996). In turn, the crown structure with low light-use efficiency may be related to the low RGR in Yaku trees.

At the whole-tree level, the tree hydraulic architecture affecting photosynthetic capacity also differed between Yaku and the other two provenances. The rate of basipetal conduit widening (β) describes how conduits widen from the treetop per unit stem length. The value of β converges to 0.2 as the predicted exponent in the WBE (West, Brown and Enquis) model in a very broad-leaved plant species. In contrast, $\beta < 0.2$ results in a decreased conduit widening rate and increased resistance to sap flow within the whole tree (Rosell et al. 2017). In the present study, β was 0.17 in Yanase, 0.13 in Yoshino, and 0.07 in Yaku (Figure 3, Table 3). These values were lower than the optimal value for water transport (0.2), which may be partly due to the need for coniferous tracheids to perform water transport and achieve mechanical stability. However, the β converges to 0.2 in the world's tallest tree species—*Sequoia sempervirens* and *Sequoiadendron giganteum* (height, 86–105 m)—suggesting the significant contribution of basipetal conduit widening as a hydraulic compensation mechanism with increasing tree height. In other words, trees that can achieve the optimal β show a higher maximum height (Williams et al. 2019). Because the size-dependence of cumulative water resistance decreases as β approaches 0.2, Yanase trees can maintain a high potential for tree growth, resulting in a high maximum height. In Yaku, β was significantly smaller than in the other two provenances, and thus tree height could be constrained as the tree size increased. In addition, there was a negative correlation between β and α (log D_h at 1 m below the treetop) in the L–D_h relationship among the three provinces (Figure 3, Table 3), suggesting that the possible hydraulic architecture of the whole tree is intraspecific constrained. If the water requirement is high (for example, if the leaf area is large), the tracheid diameter at the treetop (α) is predicted to be large even at the same stem length (Olson et al. 2021). The advantage of a high α would be that a large tracheid diameter can be maintained, such that the crown can have high water demand even in the upper part of the stem. Indeed, foliar branches were concentrated at relatively high positions in Yaku, whereas Yanase and Yoshino had a wide and sparse distribution deep into the stem (Table 2). We found that the higher β in Yanase was related to the long vertical distribution of foliar branches along the stem (Figure 3). Thus, whole-tree hydraulic architecture—as explained by axial variation in the hydraulically-weighted tracheid diameter—can be linked to leaf distribution with respect to light use strategies as well as water transport capacity, leading to differences in growth characteristics among provenances. In the present study, only trees originating from Pacific regions with high precipitation were used. However, comparisons with provenances with low precipitation may also be helpful in understanding the wider patterns of variation in the functional traits of a tree species.

Interestingly, although there were evident differences in the tree hydraulic structure, the potential transpiration rate per unit sapwood area (E_p) did not differ significantly among the provenances (Table 2). Despite having the lowest β value, Yaku had the lowest tree height, that is, a shorter L and less cumulative resistance of the whole tree. As a result, the potential specific xylem conductance (K_{ap}) was higher in Yaku trees than in Yanase and Yoshino; however, this was offset by a smaller water potential gradient from the roots to the treetop ($\Psi_R - \Psi_{TT}$). It remains to be seen whether E_p is constant in response to the growth environment, or whether it just happens to be constant as a result of the integration of genetic trait differences in each provenance. Future comparative studies on growth-related traits are required at the leaf and whole-tree levels in native habitats.

Conclusion

C. japonica is geographically widespread in Japan. In this species, intraspecific variation in growth characteristics in field-grown adult trees is regulated by whole-tree properties. Leaf traits were similar among the provenances in the same environments; nevertheless, in provenances whose native habitats were most similar to the common garden used in the present study, resource-acquisitive leaf traits were achieved through a combination of the high nutrient acquisition capacity of roots. Furthermore, the high rate of basipetal conduit widening was correlated with the long crown depth, suggesting that the light capture strategies at the whole-tree level are coordinated with hydraulic architectures, possibly to achieve the optimal growth rate for each provenance. Based on our findings, we suggest that of the mechanisms underlying intraspecific variation in the growth characteristics of trees with a wide range of native habitats can be a useful indicator for predicting changes in growth potential and forest dynamics in response to climate change in each habitat.

Acknowledgements

We thank Dr. T. Ohta, and staff members of Wakayama Experimental forest, Hokkaido University, for help of field measurement on this study. The present study was conducted using Cooperative Research Facilities (Isotope Ratio Mass Spectrometer) of Center for Ecological Research, Kyoto University. This research was funded by JSPS KAKENHI Grant Number to TH (21H02227 and 21H05316) and JSPS Research Fellowships for Young Scientists to WAA (17J05154) and KK (20J01359).

Conflict of interest

None declared.

References

Anfodillo T, Carraro V, Carrer M, et al (2006) Convergent tapering of xylem conduits in different woody species. New Phytologist 169:279–290. doi: 10.1111/j.1469-8137.2005.01587.x

Anfodillo T, Petit G, Crivellaro A (2013) Axial conduit widening in woody species: A still neglected anatomical pattern. IAWA Joural 34:352–364. doi: 10.1163/22941932-00000030

Arenas-Navarro, M., Oyama, K., García-Oliva, F., Torres-Miranda, A., De La Riva, E. G. & Terrazas, T. (2021) The role of wood anatomical traits in the coexistence of oak species along an environmental gradient. AoB PLANTS, 13, 6, 1–14. doi: 10.1093/aobpla/plab066

Asner GP, Martin RE, Tupayachi R, et al (2014) Amazonian functional diversity from forest canopy chemical assembly. Proceedings of the National Academy of Sciences of the United States of America 111:5604–5609. doi: 10.1073/pnas.1401181111

Azuma W, Ishii HRR, Kuroda K, Kuroda K (2016) Function and structure of leaves contributing to increasing water storage with height in the tallest *Cryptomeria japonica* trees of Japan. Trees—Structure and Function 30:141–152. doi: 10.1007/s00468-015-1283-3

Bartoń K (2016) MuMIn: Multi-Model Inference. R package version 1.43.17.

Bates D, Mächler M, Bolker BM, Walker SC (2015) Fitting linear mixed-effects models using lme4. Journal of Statistical Software 67:1–48. doi: 10.18637/jss.v067.i01

Brodribb TJ (2009) Xylem hydraulic physiology: The functional backbone of terrestrial plant productivity. Plant Science 177:245–251. doi: 10.1016/j.plantsci.2009.06.001

Brodribb TJ, Feild TS (2000) Stem hydraulic supply is linked to leaf photosynthetic capacity: evidence from New Caledonian and Tasmanian rainforests. Plant, Cell & Environment 23:1381–1388. doi: 10.1046/j.1365-3040.2000.00647.x

Cavender-Bares J (2019) Diversification, adaptation, and community assembly of the American oaks (Quercus), a model clade for integrating ecology and evolution. New Phytologist 221:669–692. doi: 10.1111/nph.15450

Coley P, Barone J (1996) Herbivory and plant defenses. The Annual Review of Ecology, Evolution, and Systematics 27:305–335. doi: 10.1146/annurev.ecolsys.27.1.305

Denne MP (1988) Definition of latewood according to Mork (1928). IAWA J 10:59–62.

Enquist BJ (2003) Cope's rule and the evolution of long-distance transport in vascular plants: Allometric scaling, biomass partitioning and optimization. Plant, Cell & Environment 26:151–161. doi: 10.1046/j.1365-3040.2003.00987.x

Fan ZX, Zhang SB, Hao GY, et al (2012) Hydraulic conductivity traits predict growth rates and adult stature of 40 Asian tropical tree species better than wood density. J Ecol 100:732–741. doi: 10.1111/j.1365-2745.2011.01939.x

Farquhar GD, Ehleringer JR, Hubick KT (1989) Carbon isotope discrimination and photosynthesis. Annu Rev Plant Physiol Plant Mol Biol 40:503–537. doi: 10.1146/annurev.pp.40.060189.002443

Forestry Agency of Japan. 2011. 2011 Forestry census. Tokyo: Forestry Agency.

Geological Survey of Japan. AIST (ed.) (2015) Seamless digital geological map of Japan 1: 200,000. May 29, 2015 version. Geological survey of Japan. (English and Japanese)

van Gelder HA, Poorter L, Sterck FJ (2006) Wood mechanics, allometry, and life-history variation in a tropical rain forest tree community. New Phytol 171:367–378. doi: 10.1111/j.1469-8137.2006.01757.x.

Gibert A, Gray EF, Westoby M, et al (2016) On the link between functional traits and growth rate: meta-analysis shows effects change with plant size, as predicted. J Ecol 104:1488–1503. doi: 10.1111/1365-2745.12594

Givnish TJ (1988) Adaptation to sun and shade: a whole-plant perspective. Australian Journal of Plant Physiology 15:63–92. doi: 10.1071/PP9880063

Grime JP, Thompson K, Hunt R, et al (1997) Integrated screening validates primary axes of specialisation in plants. Oikos 79:259–281. doi: 10.2307/3546011

Hacke UG, Spicer R, Schreiber SG, Plavcová L (2017) An ecophysiological and developmental perspective on variation in vessel diameter. Plant, Cell & Environment 40: 831-845. doi: 10.1111/pce.12777

Hietz P, Rosner S, Hietz-Seifert U, Wright SJ (2017) Wood traits related to size and life history of trees in a Panamanian rainforest. New Phytologist 213:170–180. doi: 10.1111/nph.14123

Hinckley TM, Duhme F, Hinckley AR, Richter H (1980) Water relations of drought hardy shrubs: osmotic potential and stomatal reactivity. Plant, Cell & Environment 3:131–140. doi: 10.1111/1365-3040.ep11580919

Hiura T, Yoshioka H, Matsunaga SN, Saito T, Kohyama TI, Kusumoto N, Uchiyama K, Suyama Y, Tsumura Y (2021) Diversification of terpenoid emissions proposes a geographic structure based on climate and pathogen composition in Japanese cedar. Scientific Reports 11:8307. doi: 10.1038/s41598-021-87810-x

Hunt R (1978) Plant growth analysis. Studies in biology no. 96. E Arnold.

Hunt R (1982) Plant growth curves. Edward Arnold, London.

Iida Y, Kohyama TS, Swenson NG, et al (2014) Linking functional traits and demographic rates in a subtropical tree community: The importance of size dependency. Journal of Ecology 102:641–650. doi: 10.1111/1365-2745.12221

Inoue Y., Kitaoka, K., Araki, M., Kenzo, T., Saito S. (2018) Seasonal changes in leaf water potential, photosynthetic and transpiration rates in upper canopy needles in *Cryptomeria japonica*. Kanto Japanese Forest Research 69: 19–22. (In Japanese with English summary).

Ishii H, Asano S (2010) The role of crown architecture, leaf phenology and photosynthetic activity in promoting complementary use of light among coexisting species in temperate forests. Ecological Research 25:715–722. doi: 10.1007/s11284-009-0668-4

Ishii H, Takashima A, Makita N, Yoshida S (2010) Vertical stratification and effects of crown damage on maximum tree height in mixed conifer-broadleaf forests of Yakushima Island, southern Japan. Plant Ecology 211:27–36. doi: 10.1007/s11258-010-9768-z

Ishii HR, Horikawa Shin-ichiro, Noguchi Y, Azuma W (2018) Variation of intra-crown leaf plasticity of *Fagus crenata* across its geographical range in Japan. Forest Ecology and Management 429:437–448. doi: 10.1016/j.foreco.2018.07.016

Itaka S, Yoshida S, Mizoue N, Ota T, Takashima A, Kajisa T, Yasue K (2013) Estimation of growth rates based on tree-ring analysis of *Cryptomeria japonica* on Yakushima

Island, Japan. Journal of Forest Planning 19:1–7. doi: 10.20659/jfp.19.1_1

Kanda T, Takata Y, Kohyama K, Ohkura T, Maejima Y, Wakabayashi S, Obara H (2018) New soil maps of Japan based on the comprehensive soil classification system of Japan – first approximation and its application to the world Reference Base for soil resources 2006. Japan Agricultural Research Quarterly 49:217–226. doi: 10.6090/jarq.52.285

King DA, Davies SJ, Tan S, Noor NSM (2006) The role of wood density and stem support costs in the growth and mortality of tropical trees. Journal of Ecology 94:670–680. doi: 10.1111/j.1365-2745.2006.01112.x

Kitajima K (1994) Relative importance of photosynthetic traits and allocation patterns as correlates of seedling shade tolerance of 13 tropical trees. Oecologia 98:419–428. doi: 10.1007/BF00324232

Kobayashi, H., Inoue, S. & Gyokusen, K. (2010) Spatial and temporal variations in the photosynthesis-nitrogen relationship in a Japanese cedar (*Cryptomeria japonica* D. Don) canopy. Photosynthetica, 48, (2), 249−256. doi: 10.1007/s11099-010-0031-6

Liu, H., Gleason, S. M., Hao, G., Hua, L., He, P., Goldstein, G. & Ye, Qing. (2019) Hydraulic traits are coordinated with maximum plant height at the global scale. Science Advances, 5, eaav1332. doi: 10.1126/sciadv.aav1332

Martínez-Vilalta J, Mencuccini M, Vayreda J, Retana J (2010) Interspecific variation in functional traits, not climatic differences among species ranges, determines demographic rates across 44 temperate and Mediterranean tree species. Journal of Ecology 98:1462–1475. doi: 10.1111/j.1365-2745.2010.01718.x

Medeiros CD, Scoffoni C, John GP, et al (2019) An extensive suite of functional traits distinguishes Hawaiian wet and dry forests and enables prediction of species vital rates. Functional Ecology 33:712–734. doi: 10.1111/1365-2435.13229

Messier J, McGill BJ, Lechowicz MJ (2010) How do traits vary across ecological scales? A case for trait-based ecology. Ecological Letter 13:838–848. doi: 10.1111/j.1461-0248.2010.01476.x

Montgomery RA, Chazdon RL (2002) Light gradient partitioning by tropical tree seedlings in the absence of canopy gaps. Oecologia 131:165–174. doi: 10.1007/s00442-002-0872-1

Moreira X, Mooney KA, Rasmann S, et al (2014) Trade-offs between constitutive and induced defences drive geographical and climatic clines in pine chemical defences. Ecological Letter 17:537–546. doi: 10.1111/ele.12253

Nabeshima E, Kubo T, Hiura T (2010) Variation in tree diameter growth in response to the weather conditions and tree size in deciduous broad-leaved trees. Forest and

Ecological Management 259:1055–1066. doi: 10.1016/j.foreco.2009.12.012

Nakagawa S, Schielzeth H (2013) A general and simple method for obtaining R^2 from generalized linear mixed-effects models. Methods Ecology and Evolution 4:133–142. doi: 10.1111/j.2041-210x.2012.00261.x

Niinemets Ü (2010) A review of light interception in plant stands from leaf to canopy in different plant functional types and in species with varying shade tolerance. Ecological Research 25:693–714. doi: 10.1007/s11284-010-0712-4

Nishizono T, Kitahara F, Iehara T, Mitsuda Y (2014) Geographical variation in age-height relationships for dominant trees in Japanese cedar (*Cryptomeria japonica* D. Don) forests in Japan. Journal of Forest Research 19:305–316. doi: 10.1007/s10310-013-0416-z

Norman J, Welles J, McDermitt D (1992) Estimating canopy light-use and transpiration efficiencies from leaf measurements. In: Inc. L-C (ed) Li-Cor Application Note #105. Lincoln, NE

Obeso JR (2002) The costs of reproduction in plants. New Phytologist 155:321–348. doi: 10.1046/j.1469-8137.2002.00477.x

Ohta T, Niwa S, Hiura T (2019) Geographical variation in Japanese cedar shapes soil nutrient dynamics and invertebrate community. Plant and Soil 437:355–373. doi:

10.1007/s11104-019-03983-5

Olson ME, Anfodillo T, Gleason SM, McCulloh KA (2021) Tip-to-base xylem conduit widening as an adaptation: causes, consequences, and empirical priorities. New Phytologist 229: 1877-1893. doi: 10.1111/nph.16961

Olson ME, Anfodillo T, Rosell JA, et al (2014) Universal hydraulics of the flowering plants: Vessel diameter scales with stem length across angiosperm lineages, habits and climates. Ecological Letter 17:988–997. doi: 10.1111/ele.12302

Olson ME, Soriano D, Rosell JA, et al (2018) Plant height and hydraulic vulnerability to drought and cold. Proceedings of the National Academy of Sciences of the United States of America 115:7551–7556. doi: 10.1073/pnas.1721728115

Onoda Y, Saluñga JB, Akutsu K, et al (2014) Trade-off between light interception efficiency and light use efficiency: Implications for species coexistence in one-sided light competition. Journal of Ecology 102:167–175. doi: 10.1111/1365-2745.12184

Osada N, Nabeshima E, Hiura T (2015) Geographic variation in shoot traits and branching intensity in relation to leaf size in Fagus crenata: a common garden experiment. American Journal of Botany 102:878–887. doi: 10.3732/ajb.1400559

Osone Y, Hashimoto S, Kenzo T (2021) Verification of our empirical understanding of the physiology and ecology of two contrasting plantation species using a trait database. PLoS One 16:274–275. doi: 10.1371/journal.pone.0254599

Parker WC, Colombo SJ (1995) A critical re-examination of pressure-volume analysis of conifer shoots: comparison of three procedures for generating PV curves on shoots of *Pinus resinosa* Ait. seedlings. Journal of Experimental Botany 46:1701–1709.

Petit G, Anfodillo T, Mencuccini M (2008) Tapering of xylem conduits and hydraulic limitations in sycamore (*Acer pseudoplatanus*) trees. New Phytologist 177:653–664. doi: 10.1111/j.1469-8137.2007.02291.x

Poorter H, Jagodzinski AM, Ruiz-Peinado R, et al (2015) How does biomass distribution change with size and differ among species? An analysis for 1200 plant species from five continents. New Phytologist 208:736–749. doi: 10.1111/nph.13571

Poorter H, Remkes C (1990) Leaf area ratio and net assimilation rate of 24 wild species differing in relative growth rate. Oecologia 83:553–559.

Poorter L, Bongers F, Sterck FJ, Wöll H (2003) Architecture of 53 rain forest tree species differing in adult stature and shade tolerance. Ecology 84:602–608.

Poorter L, Bongers L, Bongers F (2006) Architecture of 54 moist forest tree species:

traits, trade-offs, and functional groups. Ecology 87:1289–1301. doi: 10.1890/07-0207.1

Poorter L, McDonald I, Alarcón A, et al (2010) The importance of wood traits and hydraulic conductance for the performance and life history strategies of 42 rainforest tree species. New Phytologist 185:481–492.

R core Team (2019) R: A language and environment for statistical computing. R Foundation for Statistical Computing.

Reich PB (2014) The world-wide ‘fast-slow’ plant economics spectrum: a traits manifesto. Journal of Ecology 102:275–301. doi: 10.1111/1365-2745.12211

Rosell JA, Olson ME, Anfodillo T (2017) Scaling of xylem vessel diameter with plant size: causes, predictions, and outstanding questions. Current Forestry Reports 3:46–59. doi: 10.1007/s40725-017-0049-0

Ryan MG, Yoder BJ (1997) Hydraulic limits to tree height and tree growth: What keeps trees from growing beyond a certain height? Bioscience 47:235–242. doi: 10.2307/1313077

Santiago LS, Goldstein G, Meinzer FC, et al (2004) Leaf photosynthetic traits scale with hydraulic conductivity and wood density in Panamanian forest canopy trees. Oecologia 140:543–550. doi: 10.1007/s00442-004-1624-1

Schindelin J, Arganda-Carreras I, Frise E, et al (2012) Fiji: an open-source platform for biological-image analysis. Nature Methods 9:676–82. doi: 10.1038/nmeth.2019

Schneider CA, Rasband WS, Eliceiri KW (2012) NIH Image to ImageJ: 25 years of image analysis. Nature Methods 9:671–675. doi: 10.1038/nmeth.2089

Shinozaki K, Yoda K, Hozumi K, Kira T (1964) A quantitative analysis of plant form-the pipe model theory I. Basic analyses. Japanese Journal of Ecology 14:97–105. doi: 10.1086/368398

Sperry JS (2003) Evolution of water transport and xylem structure. International Journal of Plant Science 164:115–S127. doi: 10.1086/368398

Sperry JS, Adler FR, Campbell GS, Comstock JP (1998) Limitation of plant water use by rhizosphere and xylem conductance: Results from a model. Plant, Cell and Environment 21:347–359. doi: 10.1046/j.1365-3040.1998.00287.x

Spicer R, Gartner BL (2001) The effects of cambial age and position within the stem on specific conductivity in Douglas-fir (*Pseudotsuga menziesii*) sapwood. Trees – Structure and Function 15:222–229. doi: 10.1007/s004680100093

Stenberg P (1996) Simulations of the effects of shoot structure and orientation on vertical gradients in intercepted light by conifer canopies. Tree Physiology 16:99–108. doi: 10.1093/treephys/16.1-2.99

Takashima A, Kume A, Yoshida S, et al (2009) Discontinuous DBH-height relationship of *Cryptomeria japonica* on Yakushima Island: Effect of frequent typhoons on the maximum height. Ecological Research 24:1003–1011. doi: 10.1007/s11284-008-0574-1

Tateishi M, Kumagai T, Suyama Y, Hiura T (2008) Differences in transpiration characteristics of Japanese beech trees, *Fagus crenata*, in Japan. Tree Physiology 30: 748-760. doi: 10.1093/treephys/tpq023

Tobita H, Kitao M, Saito T, Kabeya D, Kawasaki T, Yazaki K, Komatsu M and Kajimoto T. (2014) Seasonal variation of photosynthetic parameters within a *Crypyomeria japonica* crown. Kanto Japanese Forest Research 65: 103–106. (In Japanese with English summary).

Tsumura Y, Uchiyama K, Moriguchi Y, et al (2012) Genome scanning for detecting adaptive genes along environmental gradients in the Japanese conifer, *Cryptomeria japonica*. Heredity (Edinb) 109:349–360. doi: 10.1038/hdy.2012.50

Tsumura Y, Uchiyama K, Moriguchi Y, et al (2014) Genetic differentiation and evolutionary adaptation in *Cryptomeria japonica*. G3 Genes|Genomes|Genetics 4:2389–2402. doi: 10.1534/g3.114.013896

Tyree MT, Hammel HT (1972) The measurement of the turgor pressure and the water relations of plants by the pressure-bomb technique. Journal of Experimental Botany 23:267–282.

Tyree MT, Zimmermann MH (2002) Xylem structure and the ascent of sap, Ed. 2. Springer-Verlag, Berlin.

West GB, Brown JH, Enquist BJ (1999) A general model for the structure and allometry of plant vascular systems. Nature 400:664–667. doi: 10.1038/23251

Williams CB, Anfodillo T, Crivellaro A, et al (2019) Axial variation of xylem conduits in the Earth's tallest trees. Trees – Structure and Function 33:1299–1311. doi: 10.1007/s00468-019-01859-w

Wright SJ, Kitajima K, Kraft NJB, et al (2010) Functional traits and the growth–mortality trade-off in tropical trees. Ecology 91:3664–3674. doi: 10.1890/09-2335.1

Wu QS, Xia RX (2006) Arbuscular mycorrhizal fungi influence growth, osmotic adjustment and photosynthesis of citrus under well-watered and water stress conditions. Journal of Plant Physiology 163:417–425. doi: 10.1016/j.jplph.2005.04.024.

Zheng, J., Li, Y., Morris, H., Vandelook, F. & Jansen, S. (2022) Variation in t racheid dimensions of conifer xylem reveals evidence of adaptation to environmental conditions. Fronters in Plant Science, 13, 774241. doi: 10.3389/fpls.2022.774241

Table 1. Comparisons of growth and relative growth rate (RGR) for height and diameter at breast heigh (DBH) in trees from 2013 to 2016, including mean values, standard errors, and the results of linear mixed model analysis for three provenances (Yaku, Yanase, and Yoshino) of *Cryptomeria japonica*. G_h: growth rate for height, Gr: growth rate for DBH, RGR_h: relative growth rate for height, RGR_r: relative growth rate for DBH.

	G_h	G_r	RGR_h	RGR_r
Unit	cm yr^{-1}	mm yr^{-1}	10^{-3} yr^{-1}	10^{-3} yr^{-1}
Yaku	5.6 (1.6) b	0.36 (0.11) b	6.08 (1.76) b	2.70 (0.80) c
Yanase	20.5 (6.1) a	1.00 (0.29) a	10.72 (3.16) a	5.60 (1.62) a
Yoshino	15.1 (4.5) a	0.95 (0.28) a	9.12 (2.72) ab	3.92 (1.14) b

Different letters indicate significant differences between parameters among provenances ($p < 0.05$).

Table 2. Comparisons of leaf, stem, and whole-tree traits among three provenances of *Cryptomeria. japonica*, including mean values, standard errors, and results of one-way ANOVA or Kruskal–Wallis test.

Trait	Symbol	Unit	Cultivars of *C. japonica*			*p* value
			Yaku	Yanase	Yoshino	
Tree structures						
Crown depth	CD	m	3.18 (0.89) b	10.89 (1.23) a	7.53 (0.80) ab	0.012
Ratio of crown depth to tree height	RCD	$m\ m^{-1}$	0.27 (0.09)	0.52 (0.08)	0.36 (0.05)	0.142
Total branch cross-sectional area per stem volume	TBA	$cm^2\ m^{-3}$	929 (170) a	594 (36) ab	439 (46) b	0.021
Sapwood density	WD	$g\ cm^{-3}$	0.39 (0.01) a	0.34 (0.01) b	0.33 (0.01) b	< 0.001
Whole-tree hydraulic architecture						
Daytime water potential of treetop leaves	Ψ_{TL}	MPa	–1.14 (0.09)	–1.33 (0.06)	–1.31 (0.06)	0.182

Daytime water potential of lowest-crown leaves	Ψ_{LL}	MPa	–1.05 (0.10)	–1.20 (0.10)	–1.24 (0.04)	0.322
Daytime water potential of fine-roots [1]	Ψ_{R}	MPa	–0.34 (0.08)	–0.20 (0.06)	–0.19 (0.01)	0.146
Water potential difference between root and treetop	$\Psi_{R} - \Psi_{TL}$	MPa	0.80 (0.13)	1.13 (0.12)	1.12 (0.05)	0.113
Axial variation-weighted potential specific xylem conductance	K_{ap}	kg m^{-2} s^{-1} MPa^{-1}	1.19 (0.06) a	0.68 (0.02) b	0.63 (0.04) b	< 0.001
Potential transpiration rate per unit sapwood area	E_p	kg m^{-2} s^{-1}	0.93 (0.13)	0.77 (0.05)	0.71 (0.06)	0.278
Leaf water relations						
Osmotic potential at turgor loss [1]	Ψ_{tlp}	MPa	–2.08 (0.20)	–1.64 (0.17)	–2.06 (0.13)	0.430
Osmotic potential at saturation [1]	Ψ_{sat}	MPa	–1.43 (0.08)	–1.09 (0.26)	–1.45 (0.02)	0.731
Relative water content at turgor loss	RWC_{tlp}	gH_2O gH_2O^{-1}	0.76 (0.03)	0.76 (0.01)	0.69 (0.02)	0.068

Leaf hydraulic capacitance	C_L	mol m^{-2} MPa^{-1}	1.52 (0.22)	1.85 (0.30)	1.94 (0.24)	0.524
Leaf succulence	S_L	gH_2O m^{-2}	204 (38)	228 (23)	241 (25)	0.687
Leaf morphology						
Leaf dry mass per area ratio [1]	LMA	g m^{-2}	411 (36)	321 (1)	385 (40)	0.061
Shoot silhouette area to projected leaf area ratio [1]	SPAR	m^2 m^{-2}	0.64 (0.01)	0.68 (0.03)	0.74 (0.05)	0.113
Leaf photosynthesis						
Maximum net photosynthetic rate	P_{max}	µmol CO_2 m^{-2} s^{-1}	3.56 (0.26)	3.17 (0.28)	4.05 (0.14)	0.095
Maximum net photosynthetic rate per leaf dry mass	P_{max_mass}	nmol CO_2 g^{-1} s^{-1}	8.69 (0.14)	9.87 (0.84)	10.76 (1.28)	0.319
Dark respiration rate [1]	R	µmol CO_2 m^{-2} s^{-1}	0.62 (0.02)	0.48 (0.09)	0.80 (0.09)	0.042
Light compensation point [1]	L_C	µmol PPFD m^{-2} s^{-1}	21.5 (1.1)	12.5 (4.9)	46.7 (12.9)	0.053
Stable carbon isotope ratio	$\delta^{13}C$	‰	–28.8 (0.27)	–29.7 (0.21)	–29.5 (0.33)	0.054

Dry-mass based carbon concentration [1]	C_{mass}	%	54.0 (0.24)	53.3 (0.35)	53.2 (0.47)	0.200
Dry-mass based nitrogen concentration	N_{mass}	%	1.10 (0.04)	1.28 (0.06)	1.21 (0.07)	0.111

Significant differences between provenances are denoted by different letters (Tukey's HSD or Steel–Dwass test, $p < 0.05$)

[1] Differences in means among provenances were examined by Kruskal–Wallis test.

Table 3. Estimation of slopes (β) and intercepts (α) for the relationships between $\log_{10}$-transformed distance from tree apex (L) and hydraulically-weighted tracheid diameter (D_h) based on the linear mixed models for three provenances (Yaku, Yanase, and Yoshino) of *Cryptomeria japonica*.

	Slope (β)	Intercept (α)
Yaku	0.070 (0.016) b	1.354 (0.012) a
Yanase	0.171 (0.023) a	1.272 (0.021) b
Yoshino	0.130 (0.022) a	1.292 (0.019) b

Values in parentheses represent standard errors.

Different letters indicate significant differences in parameters among provenances ($p < 0.05$).

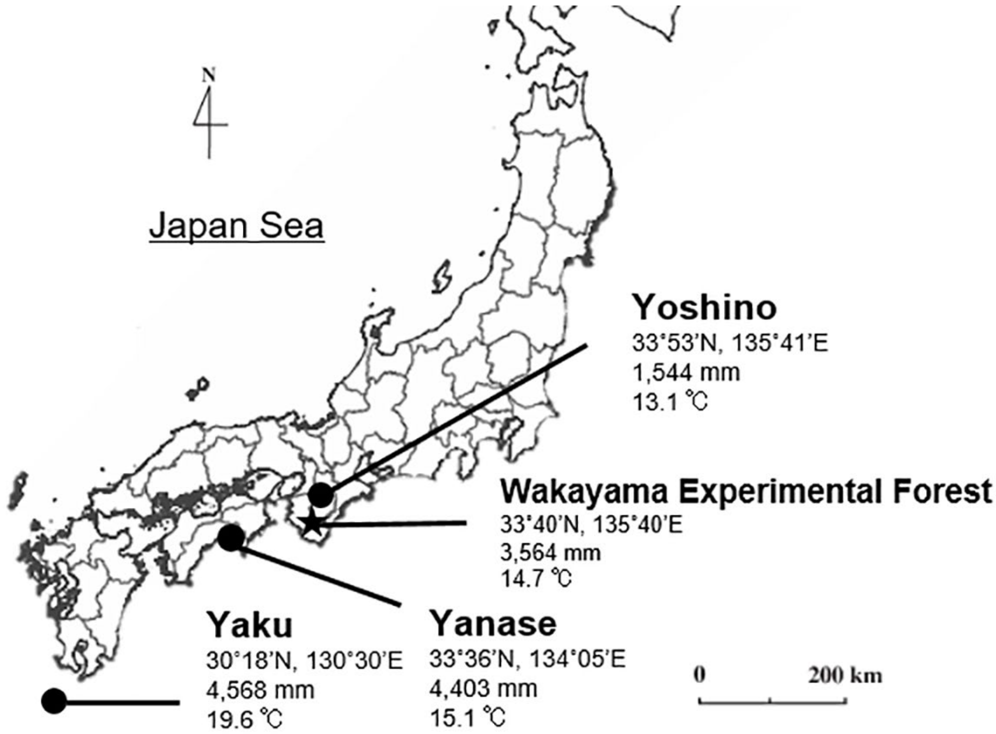

Figure 1. Location (latitude and longitude), mean annual temperature, and mean annual precipitation of the common garden of the present study (Wakayama Experimental Forest) and the native habitats of three provenances (Yoshino, Yanase, and Yaku). The location of the native habitats of three provenances shows the source location of each sapling planted in the common garden. The mean annual temperature and precipitation were calculated from observations from 1985 to 2019 at the nearest Japan Meteorological Agency weather station to that location.

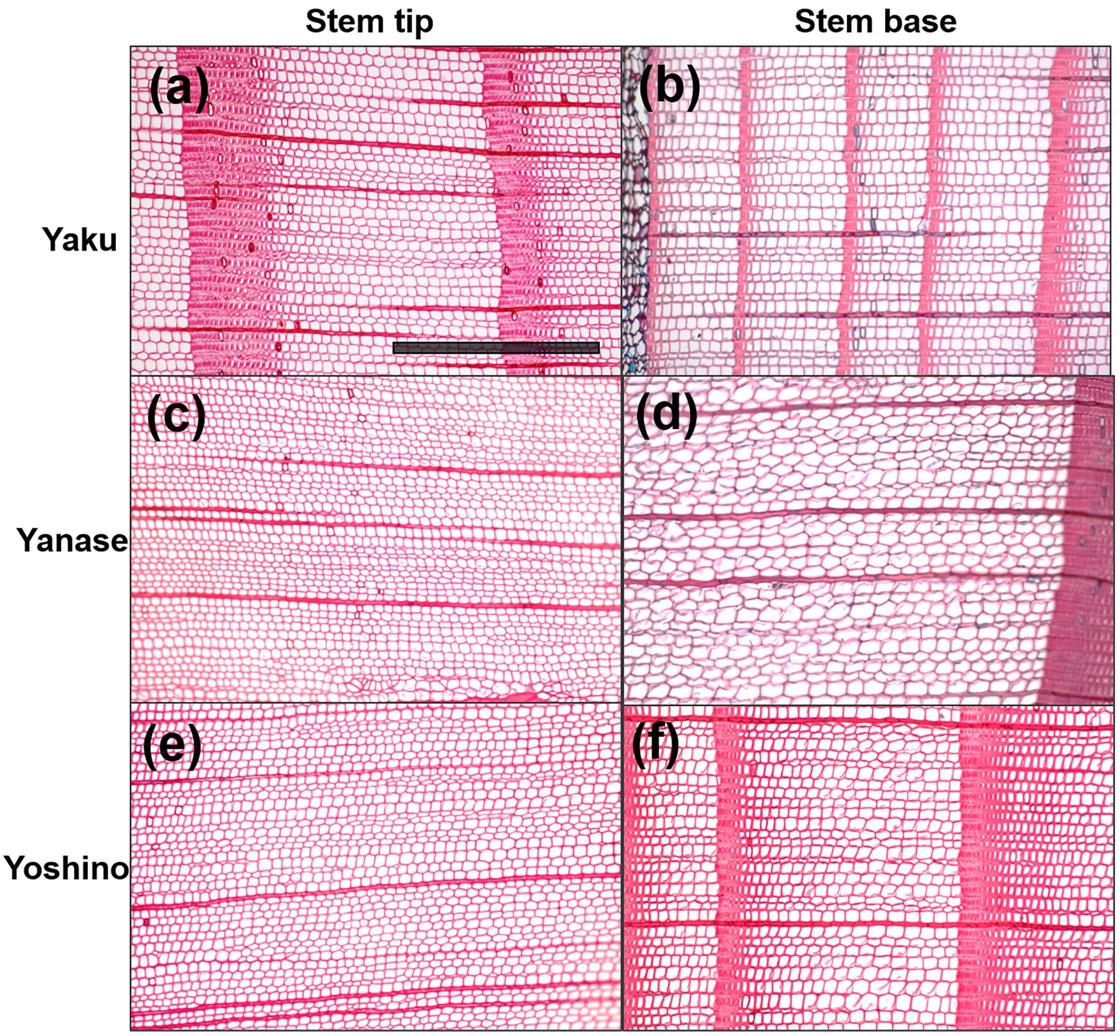

Figure 2. Optical microscopic images of stained transverse sections of the xylem at the stem tips (a, c, e) and bases (b, d, f) of three provenances of *Cryptomeria japonica*: Yaku (a, b), Yanase (c, d), and Yoshino (e, f). All images are at the same magnification (bar = 500 µm). The pith is on the right side in each image.

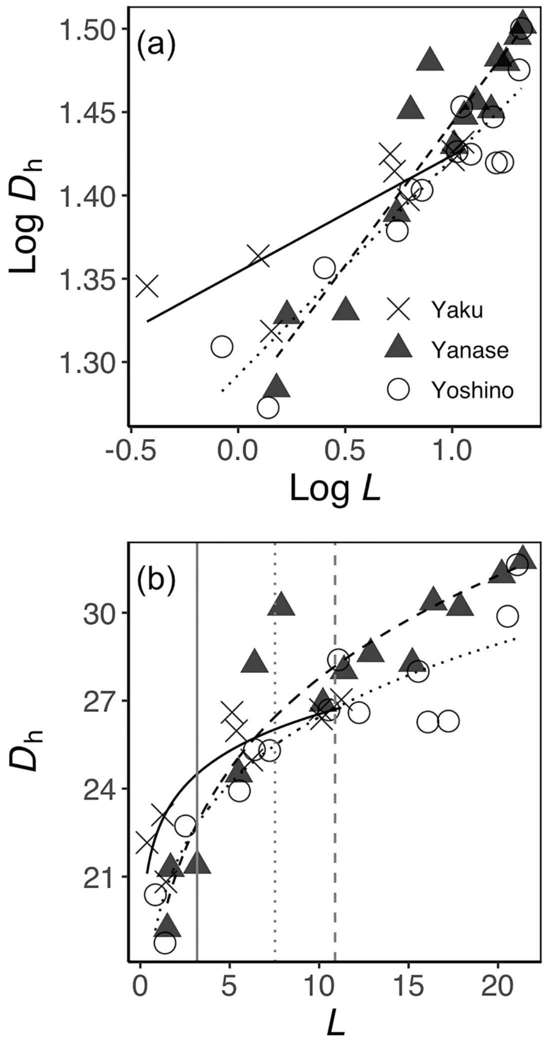

Figure 3. (a) Scaling relationships between $\log_{10}$-transformed hydraulically-weighted tracheid diameter (D_h) and distance from tree apex (L) for three provenances (Yaku, Yanase, and Yoshino) of *Cryptomeria japonica*. Solid, dashed, and dotted lines indicate the trends for Yaku, Yanase, and Yoshino, respectively. On average, the provenance with a steeper slope (β) had a longer crown depth (CD) (R^2 = 0.999, p = 0.021, n = 3). (b) The same data in non-transfomed axes. The vertical solid, dashed, and dotted lines indicate the aveage CD (see also Table 1) for Yaku, Yanase, and Yoshino, respectively. Each symbol is a composite of multiple individuals (n = 3 for each provenance).